

Origin of Lithiophilicity of Lithium Garnets: Compositing or Cleaning?

Hongpeng Zheng, Guoyao Li, Runxin Ouyang, Yao Han, Hong Zhu, Yongmin Wu, Xiao Huang, Hezhou Liu, and Huanan Duan*

Garnet-type $\text{Li}_{6.5}\text{La}_3\text{Zr}_{1.5}\text{Ta}_{0.5}\text{O}_{12}$ (LLZTO), a promising solid-state electrolyte, is reported to exhibit lithiophobicity. Herein, it is demonstrated that the origin of the lithiophobicity is closely related to the surface compositions of both the lithium and LLZTO. Surface impurities with high melting points such as Li_2O , Li_2CO_3 , LiOH , or LiF inhibit the wettability between lithium metal and LLZTO, and the widely adopted compositing strategy may improve the wettability by merely breaking the surface impurity layers. A simple but effective “polishing-and-spreading” strategy is proposed to remove the surface impurities and obtain clean Li/LLZTO interfaces. Thus, a tight and continuous Li/LLZTO interface with an interfacial resistance of $17.5 \Omega \text{ cm}^2$ is achieved, which leads to stable cycling of the symmetric Li cells and a critical current density up to 2.8 mA cm^{-2} . This work provides a new perspective to understand the lithiophilicity of garnet-type electrolytes and contributes to designing robust Li/garnet interfaces.

1. Introduction

In developing electric vehicles and large energy storage devices, rechargeable lithium batteries with high capacity, high energy


H. Zheng, G. Li, H. Liu, H. Duan
State Key Laboratory of Metal Matrix Composites
School of Materials Science and Engineering
Shanghai Jiao Tong University
Shanghai 200240, P. R. China
E-mail: hd1@sjtu.edu.cn

R. Ouyang, H. Zhu
University of Michigan-Shanghai Jiao Tong University Joint Institute
Shanghai Jiao Tong University
Shanghai 200240, China

Y. Han
Instrumental Analysis Center of SJTU
Shanghai Jiao Tong University
Shanghai 200240, P. R. China

Y. Wu
State Key Laboratory of Space Power Technology
Shanghai Institute of Space Power-Sources
Shanghai 200245, P. R. China

X. Huang
SZU-NUS Collaborative Innovation Center for Optoelectronic Science & Technology
International Collaborative Laboratory of 2D Materials for Optoelectronics Science and Technology of Ministry of Education
Institute of Microscale Optoelectronics
Shenzhen University
Shenzhen 518060, P. R. China

 The ORCID identification number(s) for the author(s) of this article can be found under <https://doi.org/10.1002/adfm.202205778>.

DOI: 10.1002/adfm.202205778

density, and long cycle life have become urgently needed. The ever-increasing energy density makes the lithium-ion battery based on lithium-ion intercalation electrodes gradually approach the theoretical limit and brings serious battery safety risks due to the flammability of liquid electrolytes. Lithium metal is the best anode because of its high theoretical specific capacity (3860 mAh g^{-1}) and low electrode potential (-3.04 V v.s. standard hydrogen electrode, SHE). Hence, by replacing the current anodes with lithium metal, one of the most promising batteries can be achieved, called the lithium metal batteries (LMBs). However, lithium dendrites could grow and penetrate the separator during plating on the lithium metal

anode, causing capacity decay and possible short circuit. One of the most attractive and practical strategies to develop LMBs is to use solid-state electrolytes (SSEs). Thus, all-solid-state lithium batteries (ASSLBs) have attracted many interests as the next high-energy-density battery. Inorganic solid electrolytes are non-flammable, non-corrosive, and extremely safe. Electric vehicles equipped with all-solid-state lithium batteries could significantly reduce the probability of catching fire. Dense solid electrolytes are believed to prevent lithium dendrites in high-energy Li-metal batteries. Among all the solid-state electrolytes, garnet-type $\text{Li}_7\text{La}_3\text{Zr}_2\text{O}_{12}$ (LLZO) is an outstanding candidate with ionic conductivity of $>10^{-4} \text{ S cm}^{-1}$, good chemical stability, and wide electrochemical windows ($>5 \text{ V}$).^[1]

However, the development of LLZO-based ASSLBs is hindered by the poor interfacial contact and considerable interfacial resistance between the Lithium and LLZO. Some researchers attribute this to the lithiophobicity of the garnet SSE material.^[2] It was reported that Li metal cannot wet garnet LLZO until heating for a long time (24–168 h) at a temperature of 300–350 °C, much higher than the Li metal melting point of 180.5 °C.^[3,4] The wettability issue will lead to uneven current distribution or current focusing across the Li/LLZO interface, which tends to cause lithium filament formation. As a result, improving the interfacial wettability is highly desirable to lower the interfacial resistance as well as inhibit the development of the lithium filament.

Various strategies, such as introducing an intermediate layer and modifying the composition of the Li anode, have been proposed to manipulate the wettability. The interlayer, such as Au,^[5] ZnO,^[6] Al_2O_3 ,^[4] SnF_2 ,^[7] AlF_3 ,^[8] hard carbon,^[9] via complex chemical and physical deposition processes, was found

to react with Li by alloying reactions and improve the interface contact. As reported by Hu and his colleagues, a 5–6 nm thick Al_2O_3 coating by atom layer deposition (ALD) decreased the interfacial ASR from 1710 ohm cm^2 to 34 ohm cm^2 . The higher binding energy of Li with lithiated alumina than that with LLZO enhances the conformal interface. The alumina provides facile Li-ion transport paths across the interface. However, growing such nano-scale layers by ALD is complex and expensive, which hinders practical applications.

Modification of Li metal itself seems another effective way to improve the wettability between Li and LLZO. The molten lithium was reported to dewet most solid substrates, such as ceramics, polymers, and even metals, due to the large difference in surface energy.^[10] By compositing to change the bonding energy, viscosity, and surface tension of the molten lithium, the surface energy of the molten Li can be tuned so that the composite can wet the LLZO. Great efforts have been dedicated to this end. Different compositing materials span from metals like Na,^[11] Mg,^[12] and nonmetallic materials like graphite,^[13] C_3N_4 ,^[14] BNNS.^[15] For instance, Duan et al. developed a lithium–graphite composite anode by mixing graphite into molten lithium, which gives an intimate contact against LLZO with an interfacial resistance of 11 $\Omega \text{ cm}^2$. The symmetric cells were cycled stably with small voltage hysteresis and enabled a critical current density up to 1 mA cm^{-2} . Such improvements were ascribed to the increased viscosity of the composite anode and interfacial reaction between the Li–C and LLZO.^[13a] Moreover, Sn was even reported as a universal soldering/alloying element to improve the wettability against different substrates, including metals, ceramics, and polymers.^[10a] However, even if the compositing strategy can be proven to be effective in the long term, which is yet to know at present, there are several obvious drawbacks of compositing: 1) additional materials cost and processing cost, 2) decreasing the specific energy of the battery because the inactive compositing materials may add mass and increase the electrode potential of the anode, and 3) compromising cycling performance unless the composite anode can maintain integrity upon cycling.^[16]

On the other hand, previous work offers a different explanation of the lithiophobicity of LLZO.^[17] The LLZO is intrinsically lithiophilic; it is the surface impurity on the LLZO that prevents the LLZO from wetting the molten Li. Several studies showed that impurities mainly consisting of Li_2CO_3 and $\text{LiOH}\cdot\text{H}_2\text{O}$ can form on the air-exposed LLZO surface as a result of a two-step process: 1) the formation of intermediate $\text{LiOH}\cdot\text{H}_2\text{O}$ due to the Li^+/H^+ exchange with the moisture in the air, and 2) the reaction of $\text{LiOH}\cdot\text{H}_2\text{O}$ with CO_2 in the air to form Li_2CO_3 .^[18] The insulating surface impurities will increase the interfacial resistance as well as inhibit the wettability with Li. Subsequently, efforts have been taken to remove the surface impurity layer on LLZO. Chen. L. et al. adopted laser cleaning to treat the garnet surface and found that the Li_2CO_3 layer was effectively reduced, and the garnet surface turned from lithiophobicity to lithiophilicity after the treatment. The resulting Li/garnet interfacial resistance was reduced from 2479.7 to 76.4 $\Omega \text{ cm}^2$ at 30 °C.^[17c] Similarly, various approaches were proposed to suppress the Li_2CO_3 formation or remove Li_2CO_3 for the air-exposed garnets, including doping,^[19] polishing and heating in an inert atmosphere,^[17b,20] and rapid acid treatment.^[21]

Our recent findings agree with the point of “intrinsic lithiophilicity” of garnet. We observed that the surface impurity layer, mainly Li_2O , on the Li metal affected its wetting with garnet. By rubbing the air-exposed garnet pellets with a 3- μm thick surface Li_2CO_3 layer on molten Li and eliminating the effect of the surface layer, a robust and stable Li/garnet interface was achieved, which enabled stable cycling of the symmetric cells without shorting. Based on these findings, it is of great interest to reconsider the origin of lithiophilicity of lithium garnets. The present work first elucidates the surface impurities to be high-melting-point salts such as Li_2O , Li_2CO_3 , LiOH , or LiF . Second, comparing the wettability between the $\text{Li}_{6.5}\text{La}_3\text{Zr}_{1.5}\text{Ta}_{0.5}\text{O}_{12}$ (LLZTO) and pure lithium/lithium-graphite (Li-C)/lithium-LLZTO (Li-LLZTO) composite anode, we demonstrate that impurities on the anode side affect the wettability more than compositing. Third, an ideal Li/garnet interface can be obtained by removing the surface impurities from both LLZTO and lithium, delivering an interface resistance as low as 17.5 $\Omega \text{ cm}^2$. The symmetric Li/LLZTO/Li cell exhibits stable cycling performance with small voltage polarization. With a simple but effective “polishing-and-spreading” strategy, the molten lithium can be quickly coated onto LLZTO as well as many other solid substrates (Fe, carbon cloth, Ni foam, and Cu foam). The present work demonstrates a promising strategy to obtain the intrinsic lithiophilicity between garnet and Li without using an intermediate layer or compositing for ASSBs.

2. Results and Discussion

The as-prepared LLZTO pellets by the solid-state reaction method exhibit a relative density of 94.5%, which was measured by the Archimedes method and based on the theoretical density of 5.4 g cm^{-3} . **Figure 1a** shows the Rietveld refinement results of $\text{Li}_{6.5}\text{La}_3\text{Zr}_{1.5}\text{Ta}_{0.5}\text{O}_{12}$ with the related refinement parameters given in Table S2 (Supporting Information). The refinement result indicates a pure cubic garnet phase without unknown diffraction peaks. The pure cubic garnet phase was rechecked by the synchrotron-based XRD implemented on the BL14B1 beamline at Shanghai Synchrotron Radiation Facility (SSRF) in Figure S1 (Supporting Information).

The tight and continuous surface contact can be obtained by coating the molten lithium onto the surface of the LLZTO pellet. Video S1 (Supporting Information) recorded the coating process in detail. The lithium metal was melted on a Ni plate at 350 °C in an Ar-filled glovebox. In the beginning, the molten lithium showed limited liquidity and was covered with a greyish and dull surficial layer (Figure S2, Supporting Information). The molten lithium in this state did not wet the LLZTO pellet when the pellet was placed on its top, similar to most previous works.^[13a,14,22] After using the tweezer to spread the molten lithium evenly on the Ni plate, the molten lithium exhibits a shining metallic luster, good fluidity, and a smooth surface (Figure S3a, Supporting Information). Then, the LLZTO pellet was put on the spread molten lithium and kept for about one minute. The molten Lithium wetted well the LLZTO surface (Figure S3b, Supporting Information).

The wetted Li-LLZTO interface was examined by SEM. The cross-sectional image in Figure 1b clearly shows a tight and

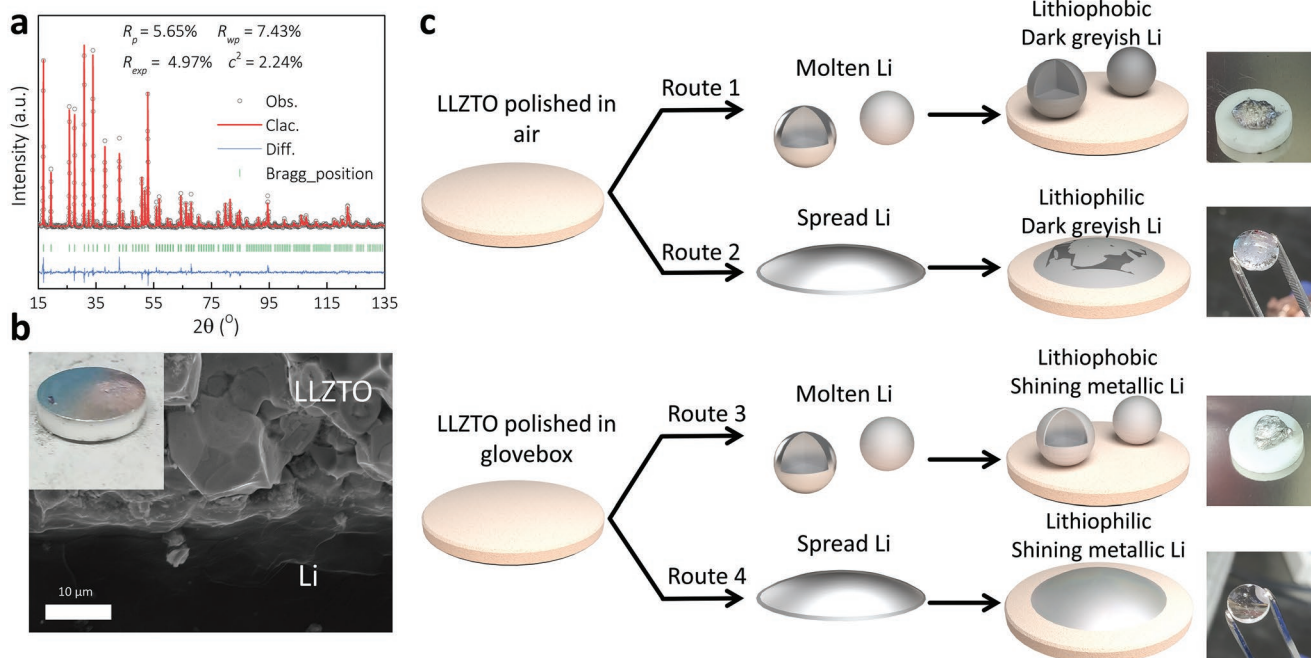


Figure 1. a) XRD patterns and the corresponding Rietveld fit ($R_{wp} = 4.97\%$) of LLZTO. Dots indicate collected data; lines through them are the model fit along with different curves shown at the bottom. The tick marks belong to the cubic garnet phase. b) Cross-sectional SEM image of the Li/LLZTO interface and the photograph of the sample in the glovebox. c) Schematic and photographs show different wetting behaviour between molten lithium and LLZTO along different routes.

continuous contact. The tight contact between the lithium metal and the LLZTO pellet largely determines the electrochemical performance, enabling a low interface resistance and high critical current density. The result in Figure 1b is in sharp comparison to previously reported results. Table S3 (Supporting Information) compiles some typical works that used modified layers or lithium alloys to improve the wettability. As shown in Table S3 (Supporting Information), when the molten lithium is directly placed on the surface of LLZTO, it looks dark greyish and non-wetting. In contrast, the present work shows that the spread molten lithium can wet various substrates such as solid Fe, porous Ni, and Cu foams, and porous carbon cloth, as shown in Figure S4 (Supporting Information).

To further explore the effects of the surface state of molten lithium and LLZTO on wetting, wettability experiments, as shown in Figure 1c, were designed and carried out. Along route 1, the LLZTO pellet was polished in the air and quickly transferred to the Ar-filled glovebox to avoid air contamination. After putting molten Li on it, it shows poor wettability with a large contact angle, and the Li surface turned dark greyish in a moment, which suggests possible reactions between the surface of the lithium metal and the garnet. Along route 2, the molten lithium was spread evenly on the Ni plate to have a smooth and shining surface. Once the polished LLZTO was put to touch the spread Li, part of the Li surface became hazy and not as glossy, implying impurities formed on the Li surface (Figure S5, Supporting Information). Meanwhile, the spread Li wets the garnet rather well. As for route 3, the LLZTO pellet was polished in the Ar atmosphere. After putting molten Li on it, the lithium

shows a metallic luster with no color change but does not wet the garnet. Along route 4, when the polished LLZTO contacts the spread molten Li, it is quickly wetted to form a mirror-like Li coating layer. The above observation clearly shows that the surfaces of the LLZTO pellet and lithium metal will jointly affect the wetting process. For LLZTO, X-ray photoelectron spectroscopy (XPS) results in Figure S6 (Supporting Information) show that the surface pollution is more severe for the LLZTO polished in air than that polished in glovebox. Previous studies also show that LLZTO surface impurities form during air exposure and the impurities can be effectively removed by mechanical polishing in glovebox.^[17a,20,23] Moreover, a small amount of moisture and carbon dioxide adsorbed by the LLZTO surface in the air will contaminate the molten lithium, as evidenced by the color change, and this can be avoided by polishing the pellets in the inert atmosphere. As for lithium metal, as long as the clean molten lithium surface is obtained, for example, by simple friction, the LLZTO electrolyte can be wetted. This obviously implies that the impurities on the Li anode play a more important role than the impurities on the LLZTO surface in determining the Li/garnet wettability.

To determine the chemical composition of the impurity layer formed on the lithium metal, XPS depth profiling was employed to characterize three types of lithium: “pristine Li”, “heated Li”, and “heated-and-contacted Li”. The “pristine Li” was a commercial lithium foil without any treatment. The “heated Li” referred to the lithium that was melted and cooled down in the Ar-filled glovebox, while the “heated-and-contacted Li” referred to the lithium that went through melting, touching the LLZTO pellet, and cooling in the Ar atmosphere. The LLZTO pellet used here was polished in the air. Since the exposure of the Li to air led

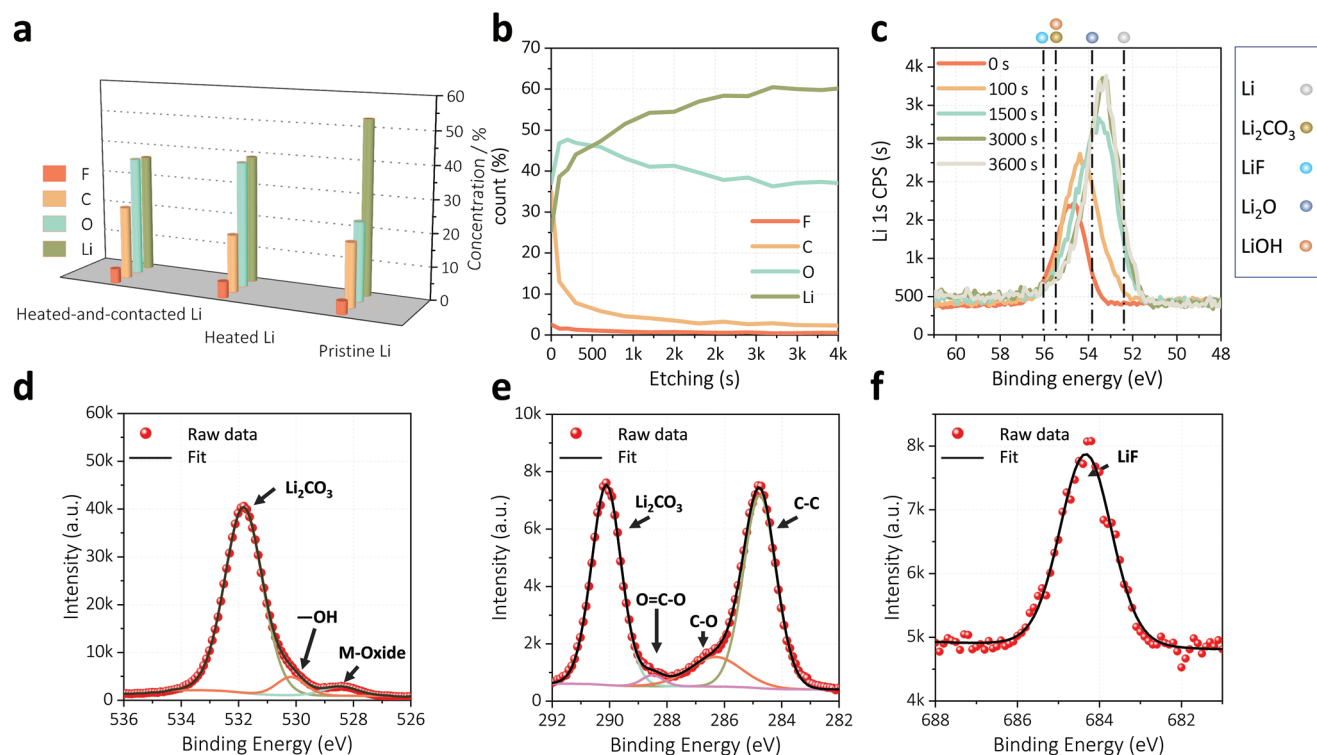


Figure 2. a) Composition comparison of the surface of pristine Li, heated-Li, and heated-and-contacted-Li samples determined via XPS after 100 s etching. b) Depth profiles of elements of the heated-and-contacted-Li sample for 4000 s etching. c) Li 1s spectra were collected from the heated-and-contacted-Li sample after 0, 100, 1500, 3000, and 3600 s etching. d–f) XPS spectra of d) O 1s, e) C 1s, and f) F 1s of the heated-and-contacted-Li sample after 100 s etching.

to almost immediate surface reactions, a method for anaerobic transfer of the sample from the glovebox to the vacuum chamber of the XPS is required. A specially designed gastight vessel filled with Ar gas was used to avoid moisture/air exposure (Figure S7, Supporting Information).

In **Figure 2a**, the compositions of surface species were extracted after 100 s etching. For pristine Li, a contaminated layer composed of C (23.92 at.%), O (19.38 at.%), and F (3.89 at.%) exists on the surface. In comparison, the amount of lithium element has decreased from 52.89 to 39.09 at.% and 36.36 at.% for the heated Li and the heated-and-contacted Li, respectively, with simultaneous increase of other impurity elements (C, O, and F). The content of the lithium element is used to evaluate the surficial purity.^[24] The higher the lithium content, the purer the lithium foil. Therefore, the surficial contamination of the heated-and-contacted Li is more severe than that of the heated Li, resulting from the contact with the LLZTO pellet, which is consistent with the observation in Figure 1c. Sharafi et al. claimed that the surface layer on LLZTO polished in the air is composed almost entirely of H, Li, C, and O by XPS.^[20] Consequently, these impurities will react and change the surface chemistry of lithium.

The source of the impurity elements (C, O, and F) in the pristine Li is mainly from the production process, which is inevitable due to the high reactivity of lithium elements. Indeed, commercial lithium is commonly passivated to reduce corrosion during storage and increase safety, and the passivation treatment usually involves wax, CO₂, polymer coatings, as well

as phosphorous and fluorinating agents.^[25] Another source of fluorine element may be the volatile organic agents containing fluorine (HF and PF₅) in the glovebox. Although the content of moisture and O₂ is carefully controlled in the glovebox, there might still be detectable reactions, especially at the temperatures investigated (350–400 °C), which is consistent with the previous results.^[26,10b,24]

Figure 2b shows the depth profile of different element contents in atomic ratio for the heated-and-contacted Li. With the etching starting from the surface into the inside of lithium foil, the element contents tend to reach a plateau. The contents of C and F display a rapid drop in the initial etching, and the contents of O and Li have a corresponding increase. After that, the contents of C and F maintain a low level, and the content of O gradually decreases but is >30 at.%. These findings show that the Li, C, O, and F elements mainly make the surface layer of the heated-and-contacted Li, and the thickness of the oxide layer is more than the analysis depth of the XPS. To further analyze the chemical composition of the surface layer, Li 1s spectra are extracted and shown in Figure 2c. With the etching time from 0 to 3600 s, the peak shifted from the high binding energy to the low. The binding energy of Li 1s is 55.9, 55.5, 53.7, and 52.3 eV for LiF, Li₂CO₃, LiOH or Li₂O, and Li, respectively.^[27] So, with the etching starting from the surface into the inside of the heated-and-contacted Li, the main impurities probably change successively from LiF, Li₂CO₃, LiOH, or Li₂O. The coexistence of more than one impurity in the surface layer leads to the peak broadening of the binding energy. Figure 2d–f shows

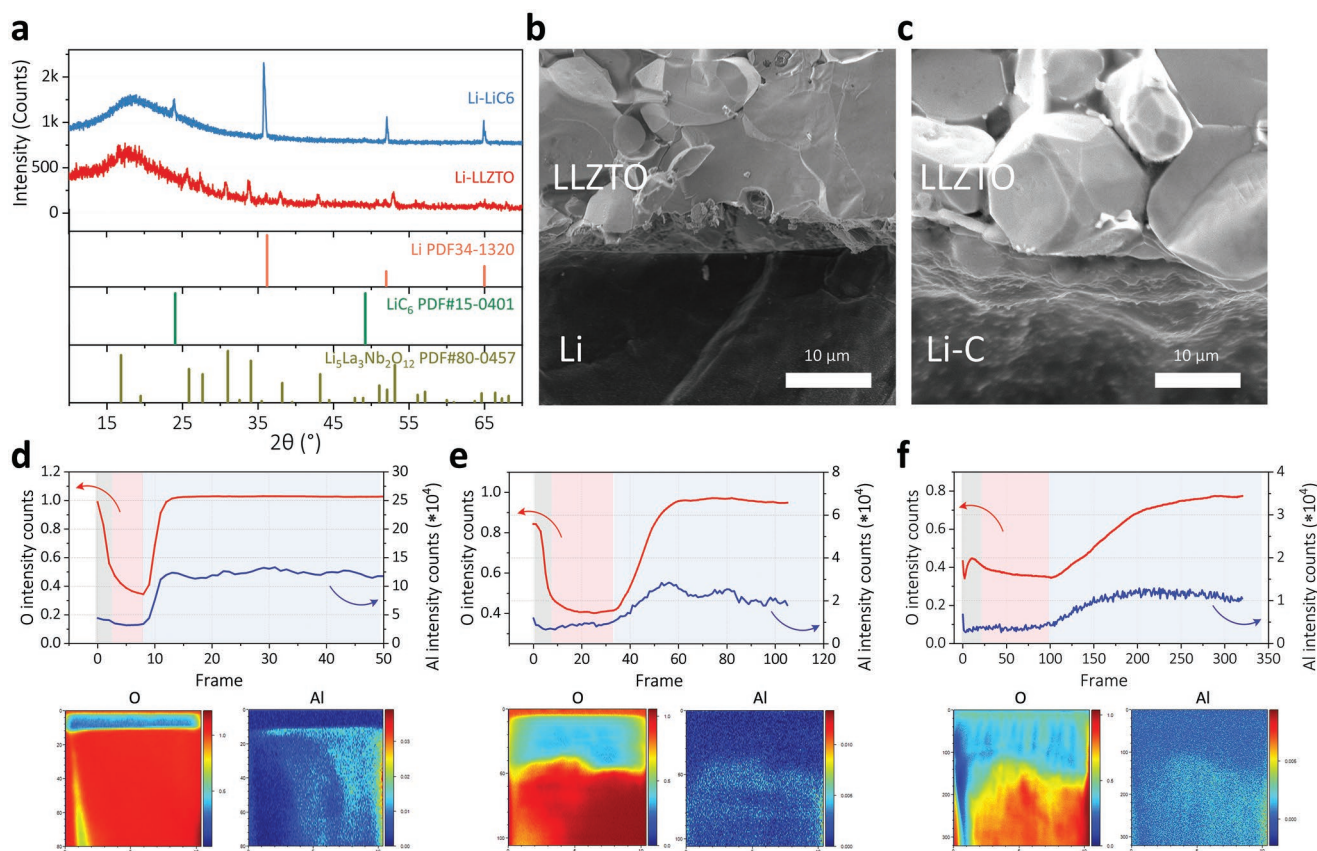


Figure 3. a) XRD pattern of the Li–C and Li–LLZTO composite anode. b–c) Cross-sectional SEM images of the b) Li–C/LLZTO and c) Li–LLZTO/LLZTO interfaces. d–f) TOF-SIMS depth profiling and the corresponding maps of d) O and Al secondary ion (SI) for the Li/LLZTO interface, e) Li–C/LLZTO interface, f) Li–LLZTO/LLZTO interface.

the spectra of O 1 s, C 1 s, and F 1 s of the heated-and-contacted Li after 100 s etching. They confirm that the impurity layer on the heated-and-contacted Li mainly consists of Li₂CO₃ or LiOH, Li₂O, and LiF.

To investigate the effects of compositing on wettability, three types of lithium-based composite anode were designed and examined. One was lithium without any additives, and the other two were lithium added with graphite and LLZTO powders, respectively. Figure 3a shows the X-ray diffraction patterns of the Li–C and Li–LLZTO composites. For the Li–C composite, the characteristic peaks of lithium (PDF#01-1131) and LiC₆ (PDF#34-1320) both occur, confirming the existence of LiC₆. For the Li–LLZTO composite, the characteristic peaks of lithium (PDF#01-1131) and garnet cubic phase (PDF#80-0457) both exist, indicating the chemical stability of LLZTO with molten lithium. From the SEM images and the EDX mapping images shown in Figure S8 (Supporting Information), LiC₆ and LLZTO particles are uniformly distributed in the lithium matrix.

Applying the above three types of the lithium-based anode, the wettability to LLZTO was surveyed and recorded in Video S2 (Supporting Information). None of them could wet the LLZTO pellet with just covering and heating on the Ni plate. In contrast, following Route 4 in Figure 1c, when the Li–C and Li–LLZTO composites were melted and spread on the Ni plate, they wet the LLZTO pellet as recorded in Videos S3-1 and S3-2

(Supporting Information), respectively. The molten Li–C composite looked greyish at first and showed a metallic luster after being spread on the Ni plate. The lithium composite in such a state easily wet the LLZTO pellet. A similar phenomenon was observed for the Li–LLZTO composite. Cross-sectional SEM images of the Li–C/LLZTO and Li–LLZTO/LLZTO interfaces are shown in Figure 3b,c, respectively. Both interfaces exhibit tight and continuous contact without any noticeable voids. These observations suggest that the LLZTO pellet exhibits lithiophobic to the melted lithium-based composite and lithiophilic to the spread one. Combining the results in Figure 1, we propose that it is the impurities on the anode surface rather than alloying or compositing that determine the wettability. This might provide a new perspective to understand the function of compositing and intermediate layer reported previously:^[4–7,11–13,14,15,22a,e,28] they improve the wettability by breaking (for alloying) or reacting (for intermediate layer) the impurity layer on the lithium surface.

Furthermore, time-of-flight secondary-ion mass spectrometry (TOF-SIMS) with depth-profiling analysis was performed to investigate the interfaces of Li/LLZTO, Li–C/LLZTO, and Li–LLZTO/LLZTO obtained by the spread technique. TOF-SIMS is a surface-sensitive technique to determine the chemical composition of buried interfaces with lithium. Due to the matrix effects, the TOF-SIMS results are only semiquantitative and

not inherently compound-specific.^[24] From the secondary ion signals of O and Al shown in Figure 3d, the Li/LLZTO interface can be divided into three regions: the top one that is O-rich and Al-poor is attributed to the impurity layer on the Li surface mainly consisting of Li₂O; the middle one that is O-poor and Al-poor area represent the lithium-based anode; and the inner one that is O-rich and Al-rich is the LLZTO pellet. The LLZTO pellet contains a certain amount of Al because the Al element coming from the alumina crucibles may enter the LLZTO pellet and help stabilize the cubic garnet structure during sintering.^[5,29] As shown in Figures 3e,f, the element distribution profiles of the Li-C/LLZTO and Li-LLZTO/LLZTO interfaces have a similar three-region structure as that of the Li/LLZTO. It should be noted that the top two regions are not as distinct in Figure 3f as in Figure 3d,e. The reason is probably that the O element in the Li-LLZTO anode is higher than those in the lithium anode and Li-C anode since 20 wt.% of LLZTO powders were added into the Li-LLZTO anode. For the top region, that is, the impurity layer, the secondary ion signals like OH⁻, CO₃²⁻ and F⁻ are also detected and shown in Figure S9 (Supporting Information), indicating more than one type of impurity existing on the surface, which is consistent with the XPS results in Figure 2. Between the anode and the LLZTO, there was no detectable impurity layer for all three interfaces, confirming the superior wettability of LLZTO to Li.

Li metal and Li-C composite were assembled into symmetric cells and subject to electrochemical evaluation. The typical Nyquist plots in Figure 4a exhibit a semicircle in the high and medium frequency region followed by a tail in the low-

frequency region. The high-frequency x -intercept of the semicircle can be attributed to the garnet resistance; the interfacial resistance (the charge transfer resistance) can be determined from the semicircle at the high and medium frequencies; the low-frequency tail may correspond to the Li⁺ diffusion.^[30] By fitting with the equivalent circuit shown in the inset of Figure 4a, the interfacial area-specific resistance (ASR) is determined by dividing the interfacial resistance by two and normalizing to the electrode surface area (0.98 cm²). The interfacial ASR of the Li/LLZTO/Li and Li-C/LLZTO/Li-C cells are 175 and 20 Ω cm², respectively. These values are much smaller than most of the previously reported values.^[22a,28b,31] Notably, the small interfacial resistances were achieved without any surface modification, which emphasizes the tight and continuous contact between the anode and the electrolyte facilitates the fast ion transport across the interface. On the other hand, there is still a slight difference in interfacial resistance, which can be attributed to the way Li-ions transport across the interface. In the Li-C anode, due to the layered structure of LiC₆, only when the LiC₆ layer is vertical to the Li-C/LLZTO interface can effectively occur Li transport across the interface. Nevertheless, the orientation of the LiC₆ in the composite anode is random, so the misorientation will inhibit the Li transport and cause high interfacial resistance.

To better understand the ion transport process, the distribution of relaxation times (DRT) analysis was employed, which transforms the impedance data from the frequency domain to the time domain so that peaks associated with characteristic relaxation times can be identified. The DRT analysis results are

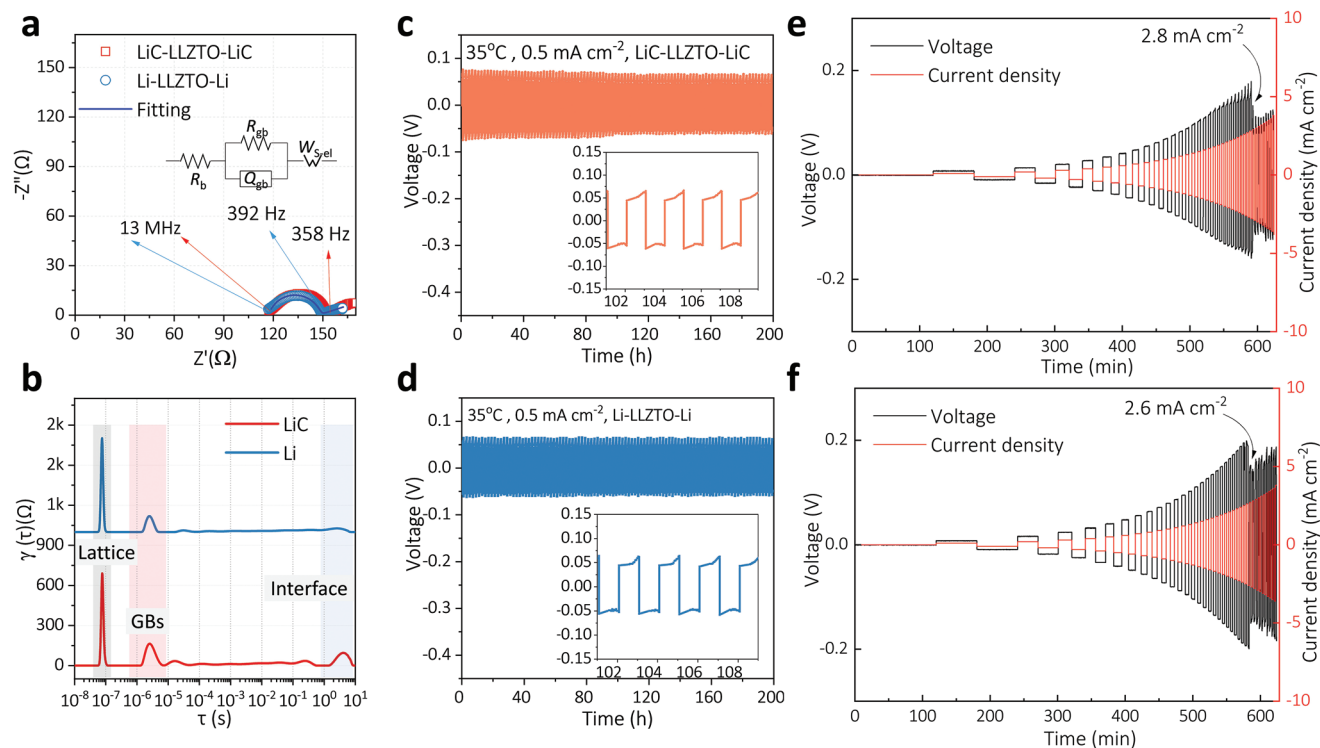


Figure 4. a) Nyquist plots and b) DRT analysis of the EIS spectra of the symmetric Li/LLZTO/Li and Li-C/LLZTO/Li-C cells. c,d) Galvanostatic cycling of the symmetric c) Li/LLZTO/Li and d) Li-C/LLZTO/Li-C cells at 0.5 mA cm⁻². e,f) Galvanostatic cycling of the symmetric Li/LLZTO/Li and Li-C/LLZTO/Li-C cells with a stripping/plating capacity of 0.1 mAh cm⁻² and ramping current density from 0.1 to 4 mA cm⁻² at room temperature.

shown in Figure 4b. The peaks in the small ($\approx 10^{-7}$ s), medium ($\approx 10^{-5}$ – 10^{-6} s), and large ($\approx 10^0$ – 10^1 s) relaxation time regions are associated with the ion transport within the garnet lattices, near the grain boundaries, and across the Li/electrolyte interface, respectively.^[32] A strong peak means large resistance and slow ion transport. Obviously, from Figure 4b, the main difference between the Li/LLZTO/Li and Li-C/LLZTO/Li-C cells is the peak corresponding to the Li/electrolyte interface. The peak intensity with the relaxation time of $\approx 10^0$ – 10^1 s is slightly larger for the Li-C/LLZTO/Li-C cell than for the Li/LLZTO/Li cell, consistent with the larger interfacial resistance for the former in Figure 4a.

The electrochemical performance of the symmetric cells was evaluated in terms of galvanostatic cycling. As shown in Figures 4c,d, both the Li/LLZTO/Li and the Li-C/LLZTO/Li-C cells exhibit stable cycling and maintain a voltage polarization of ≈ 0.017 V for 200 h at a relatively high current density of 0.5 mA cm^{-2} at 35°C . The areal capacity is maintained to be 0.5 mAh cm^{-2} throughout the tests. From the voltage profile of each cycle (insets in Figures 4c,d), the voltage increases in the positive half cycle corresponding to the Li dissolution and decreases in the negative half cycle corresponding to the Li plating, suggesting no sign of short circuit. It should be noted that the resistances estimated by the Ohm's law in Figures 4c,d are smaller than those by the Nyquist plots in Figure 4a, which can be attributed to the activation process of the Li/LLZTO interfaces and a certain degree of penetration of the plated lithium into the ceramic electrolyte.⁶ Post-test morphology study in Figures S11 and S12 (Supporting Information) shows that on the plating side, a $\approx 2.5 \mu\text{m}$ thick lithium layer forms between the anode and LLZTO, which corresponds to the plating capacity of 0.5 mAh cm^{-2} ; on the stripping side, voids are present in the lithium electrode as a result of insufficient mass transport of lithium atom, causing the polarization increase. It is noted from Figure S12 c,d (Supporting Information) that the plated lithium has very low carbon content by the element distribution analysis, which implies that the plated lithium is pure lithium rather than Li-C.

Moreover, the critical current density (CCD), which is defined as the maximum current density of an electrolyte that can withstand before shorting, was determined with the method reported previously.^[17b] As shown in Figures 4e,f, with the ramping current density, the charge-discharge voltage increases accordingly till a sudden decrease occurs, indicating the appearance of shorting. The CCD of the Li/LLZTO/Li and the Li-C/LLZTO/Li-C cells were determined to be 2.8 and 2.6 mA cm^{-2} , respectively. These CCD values are among the highest reported values, emphasizing that the lithiophilicity of LLZTO with the spread lithium-based anode endows excellent Li-ion transport property across the Li/garnet interface.

To further demonstrate the effectiveness of the “polished-and-spreading” strategy, the as-prepared Li/LLZTO stacks were coupled with three types of cathodes to assemble Li/LLZTO/LFP (LiFePO₄), Li/LLZTO/NMC (LiNi_{0.8}Co_{0.1}Mn_{0.1}O₂) and Li/LLZTO/S (sulfur) cells. A small amount ($\approx 15 \mu\text{L}$) of liquid electrolyte was added to wet the interface between the cathode and LLZTO. As shown in Figure S13 (Supporting Information), these full cells with the spread Li anode demonstrated decent

specific capacity and good cycle stability. Take Li/LLZTO/LFP as an example, at 1 C (0.51 mA cm^{-2}), the discharge capacity in the first and 50th cycle is 155.0 and 150.9 mAh g^{-1} , respectively, implying excellent capacity retention. This shows good compatibility of the “polished-and-spreading” strategy.

To understand the lithiophilicity of LLZTO, the interface formation energies (γ) of LLZTO (001)/Li (001), LLZTO (001)/LiOH (010), LLZTO (001)/LiF (001), LLZTO (001)/LiC₆ (110), LLZTO (001)/Li₂CO₃(001), and LLZTO (001)/Li₂O (001) systems were calculated by first-principle calculations. The interface formation energy is the energy difference between an interface system and the isolated components. $\gamma = (E_{a/b} - N_a \times E_a - N_b \times E_b) / 2S$, where $E_{a/b}$ refers to the total energy of the interface model; N_a and N_b refer to the formula unit number of a and b , respectively; E_a and E_b refer to the bulk energy per formula unit of a and b , respectively; S refers to the interfacial area, and 2 accounts for the existence of two interfaces in the interface system.^[33]

As illustrated in Figure 5a–g, the γ for the LLZTO/LiOH, LLZTO/LiF, LLZTO/Li₂CO₃, LLZTO/Li₂O, LLZTO/LiC₆, and LLZTO/Li interfaces is ≈ 1.53 , 0.45, 3.19, 0.53, -0.55 , and -6.19 J m^{-2} , respectively. The negative value of γ means that the interface system tends to spontaneously form and be thermodynamically stable, and the tendency has a positive correlation with the absolute value of γ , so the γ can be used to describe the wettability of different Li-containing materials. The wettability to LLZTO follows the order: Li > LiC₆ > LiF > Li₂O > LiOH > Li₂CO₃. According to the calculation results, only the lithium metal and Li-C alloy have intrinsic wettability, whereas the impurities like LiF, Li₂O, LiOH, and Li₂CO₃ are not able to wet LLZTO, which is consistent with the previous experiments.^[17a,20,34] Moreover, as shown in Figures 5e,f, the γ for the LLZTO/Li interface is as low as -6.19 J m^{-2} , which is more negative than that of the LLZTO/LiC₆ interface, implying that Li can form a stable anode/garnet interface more favorably than LiC₆, or the graphite will impair, not enhance, the wettability between LLZTO and Li. This is consistent with the interfacial ASR results of the LLZTO/Li ($17.5 \Omega \text{ cm}^2$) and LLZTO/LiC₆ interfaces ($20 \Omega \text{ cm}^2$) in Figure 4a. In contrast, the LiF, LiOH, and Li₂CO₃ do not wet LLZTO, which confirms that it is the impurity layer on the Li surface that hinders the lithiophilicity. As for whether metal lithium needs to be composited with graphite, it will not change the wettability but will reduce the ion transport across the interface.

Figure 5h summarizes the above experimental and computational results and describes the lithiophobicity and lithiophilicity of LLZTO with molten Li. Figure 2 shows that the surface impurities on Li usually consist of Li₂O, Li₂CO₃, LiOH, or LiF. There are three possible sources of these impurities. First, during the production and transportation of the lithium foil, partial oxidation, and residues of impurities such as paraffin inevitably exist on the lithium surface. Second, during heating in the glovebox, lithium metal may react rapidly with volatile organics (i.e., PF₅) in the glovebox. Third, the adsorbed gas molecules (i.e., CO₂, H₂O) or the impurity layer (i.e., Li₂CO₃) on the LLZTO surface might contaminate the lithium surface. These impurities, despite the small amount, are not able to wet LLZTO because all of them show positive interface formation

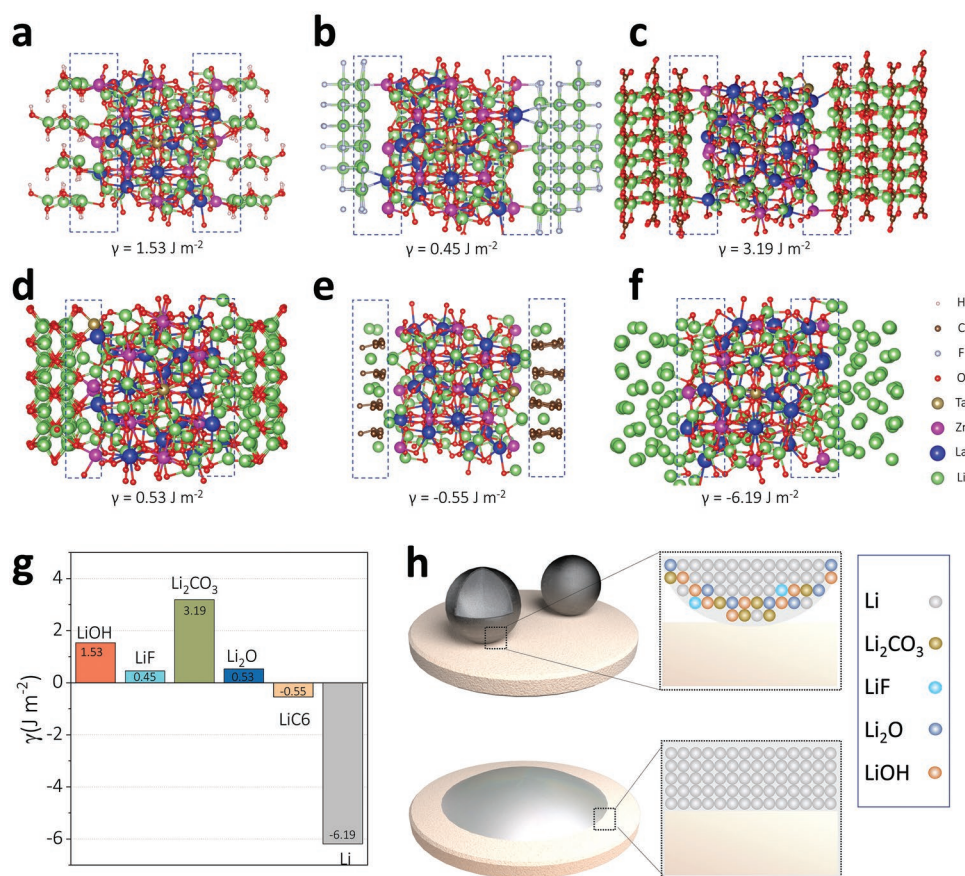


Figure 5. a–f) The optimized interface models of a) LLZTO/LiOH, b) LLZTO/LiF, c) LLZTO/Li₂CO₃, d) LLZTO/Li₂O, e) LLZTO/LiC₆, and f) LLZTO/Li for first-principle calculations. g) Comparison of the interface formation energies of LLZTO with different surfaces. h) Schematic of lithiophobicity and lithiphilicity of LLZTO with molten Li.

energy with LLZTO, as shown in Figure 5. In contrast, the γ for the LLZTO/Li interface is as low as -6.19 J m^{-2} . This implies that it is the impurity layer on the Li surface that hinders the lithiphilicity. By spreading the molten Li on a heating plate, impurities originally formed on the Li surface are broken by the shear force so that fresh molten lithium can directly contact LLZTO. Thanks to the intrinsic lithiphilicity of LLZTO, it will show good wetting behavior and form intimate Li/LLZTO interface, as evidenced in Figure 1c. Moreover, these impurity layers can be effectively eliminated by polishing the LLZTO pellets in the glovebox and spreading the molten Li on a heating plate. Once the clean surfaces are obtained, the LLZTO displays excellent wettability to the molten Li or lithiphilicity, which results in intimate Li/LLZTO interface contact, low interfacial resistance, high CCD, and stable cycling, as shown in Figures 3 and 4. The present understanding, on the one hand, stresses that the often-neglected surface impurities on the Li anode play an important role in determining wettability. On the other hand, it provides an alternative viewpoint to interpret the function of the heavily researched strategies of compositing or introducing intermediate layers. They might turn lithiophobic garnet into lithiphilic by either breaking (for compositing) or reacting (for intermediate layer) the impurity layer on the lithium surface. Furthermore, a simple but effective “polishing-and-spreading” strategy is proposed to completely avoid the possible drawbacks

involved in compositing or using intermediate layers by cutting additional materials and processing costs and preventing cell energy loss, which is important to consider when designing future garnet-based ASSLBs.

3. Conclusions

In summary, we have demonstrated that the origin of the lithiophobicity of a garnet-type LLZTO is closely related to the surface impurities of both the lithium and LLZTO. Experimental analysis and theoretical calculations show that the surface impurities usually consist of Li₂O, Li₂CO₃, LiOH, or LiF, which, despite the small amount, inhibit the wettability between lithium metal and LLZTO. Comparative study of the wetting behavior of pure lithium, Li–C and, Li–LLZTO composite anode implies that the effectiveness of the heavily researched strategies of compositing or introducing intermediate layers may be due to breaking the surface impurity layers. Furthermore, a simple but effective “polishing-and-spreading” strategy was proposed to obtain clean Li/LLZTO interfaces, which provides an interfacial resistance of $17.5 \text{ } \Omega \text{ cm}^2$ and a critical current density up to 2.8 mA cm^{-2} . This work sheds light on understanding the lithium/solid electrolyte interfaces and contributes to designing garnet-based ASSLBs.

Supporting Information

Supporting Information is available from the Wiley Online Library or from the author.

Acknowledgements

This work was financially supported by the National Natural Science Foundation of China (no. 51972211) and the Shanghai Aerospace Advanced Technology Joint Research Fund (USCAST2020-32). Instrumental Analysis Center of SJTU and National Engineering Research Center for Nanotechnology are gratefully acknowledged for assisting with relevant experimental analysis. The Center for High-Performance Computing of SJTU is gratefully acknowledged for providing computational facilities for all the simulations.

Conflict of Interest

The authors declare no conflict of interest.

Data Availability Statement

The data that support the findings of this study are available from the corresponding author upon reasonable request.

Keywords

CCD, composite anodes, interfacial impedance, LLZO, surface impurities, wettability

Received: May 20, 2022

Revised: July 12, 2022

Published online: August 5, 2022

- [1] H. Zheng, G. Li, J. Liu, S. Wu, X. Zhang, Y. Wu, H. Zhu, X. Huang, H. Liu, H. Duan, *Energy Storage Mater.* **2022**, 49, 278.
- [2] Z. Huang, L. Chen, B. Huang, B. Xu, G. Shao, H. Wang, Y. Li, C.-A. Wang, *ACS Appl. Mater. Interfaces* **2020**, 12, 56118.
- [3] J. Wolfenstine, J. L. Allen, J. Read, J. Sakamoto, *J. Mater. Sci.* **2013**, 48, 5846.
- [4] X. Han, Y. Gong, K. Fu, X. He, G. T. Hitz, J. Dai, A. Pearse, B. Liu, H. Wang, G. Rubloff, Y. Mo, V. Thangadurai, E. D. Wachsman, L. Hu, *Nat. Mater.* **2017**, 16, 572.
- [5] C.-L. Tsai, V. Roddatis, C. V. Chandran, Q. Ma, S. Uhlenbruck, M. Bram, P. Heitjans, O. Guillon, *ACS Appl. Mater. Interfaces* **2016**, 8, 10617.
- [6] C. Wang, Y. Gong, B. Liu, K. Fu, Y. Yao, E. Hitz, Y. Li, J. Dai, S. Xu, W. Luo, E. D. Wachsman, L. Hu, *Nano Lett.* **2017**, 17, 565.
- [7] B. Hu, W. Yu, B. Xu, X. Zhang, T. Liu, Y. Shen, Y.-H. Lin, C.-W. Nan, L. Li, *ACS Appl. Mater. Interfaces* **2019**, 11, 34939.
- [8] T. Wang, J. Duan, B. Zhang, W. Luo, X. Ji, H. Xu, Y. Huang, L. Huang, Z. Song, J. Wen, C. Wang, Y. Huang, J. B. Goodenough, *Energy Environ. Sci.* **2022**, 15, 1325.
- [9] L. Chen, J. Zhang, R.-A. Tong, J. Zhang, H. Wang, G. Shao, C.-A. Wang, *Small* **2022**, 18, 2106142.
- [10] a) C. Wang, H. Xie, L. Zhang, Y. Gong, G. Pastel, J. Dai, B. Liu, E. D. Wachsman, L. Hu, *Adv. Energy Mater.* **2018**, 8, 1701963; b) S.-H. Wang, J. Yue, W. Dong, T.-T. Zuo, J.-Y. Li, X. Liu, X.-D. Zhang, L. Liu, J.-L. Shi, Y.-X. Yin, Y.-G. Guo, *Nat. Commun.* **2019**, 10, 4930; c) L. Chen, G. Chen, W. Tang, H. Wang, F. Chen, X. Liu, R. Ma, *Mater. Today Energy* **2020**, 18, 100520.
- [11] X. Fu, T. Wang, W. Shen, M. Jiang, Y. Wang, Q. Dai, D. Wang, Z. Qiu, Y. Zhang, K. Deng, Q. Zeng, N. Zhao, X. Guo, Z. Liu, J. Liu, Z. Peng, *Adv. Mater.* **2020**, 32, 2000575.
- [12] K. Fu, Y. Gong, Z. Fu, H. Xie, Y. Yao, B. Liu, M. Carter, E. Wachsman, L. Hu, *Angew. Chem., Int. Ed.* **2017**, 56, 14942.
- [13] a) J. Duan, W. Wu, A. M. Nolan, T. Wang, J. Wen, C. Hu, Y. Mo, W. Luo, Y. Huang, *Adv. Mater.* **2019**, 31, 1807243; b) J. Duan, Y. Zheng, W. Luo, W. Wu, T. Wang, Y. Xie, S. Li, J. Li, Y. Huang, *Natl. Sci. Rev.* **2020**, 7, 1208.
- [14] Y. Huang, B. Chen, J. Duan, F. Yang, T. Wang, Z. Wang, W. Yang, C. Hu, W. Luo, Y. Huang, *Angew. Chem., Int. Ed.* **2020**, 59, 3699.
- [15] J. Wen, Y. Huang, J. Duan, Y. Wu, W. Luo, L. Zhou, C. Hu, L. Huang, X. Zheng, W. Yang, Z. Wen, Y. Huang, *ACS Nano* **2019**, 13, 14549.
- [16] Z. Tong, S.-B. Wang, Y.-K. Liao, S.-F. Hu, R.-S. Liu, *ACS Appl. Mater. Interfaces* **2020**, 12, 47181.
- [17] a) J.-F. Wu, B.-W. Pu, D. Wang, S.-Q. Shi, N. Zhao, X. Guo, X. Guo, *ACS Appl. Mater. Interfaces* **2019**, 11, 898; b) H. Zheng, S. Wu, R. Tian, Z. Xu, H. Zhu, H. Duan, H. Liu, *Adv. Funct. Mater.* **2020**, 30, 1906189; c) L. Chen, Y. Su, J. Zhang, H. Zhang, B. Fan, G. Shao, M. Zhong, C.-A. Wang, *ACS Appl. Mater. Interfaces* **2021**, 13, 37082.
- [18] a) H. Duan, H. Zheng, Y. Zhou, B. Xu, H. Liu, *Solid State Ionics* **2018**, 318, 45; b) W. Xia, B. Xu, H. Duan, X. Tang, Y. Guo, H. Kang, H. Li, H. Liu, *J. Am. Ceram. Soc.* **2017**, 100, 2832.
- [19] Y. Li, B. Xu, H. Xu, H. Duan, X. Lü, S. Xin, W. Zhou, L. Xue, G. Fu, A. Manthiram, J. B. Goodenough, *Angew. Chem., Int. Ed.* **2017**, 56, 753.
- [20] A. Sharafi, E. Kazyak, A. L. Davis, S. Yu, T. Thompson, D. J. Siegel, N. P. Dasgupta, J. Sakamoto, *Chem. Mater.* **2017**, 29, 7961.
- [21] H. Huo, Y. Chen, N. Zhao, X. Lin, J. Luo, X. Yang, Y. Liu, X. Guo, X. Sun, *Nano Energy* **2019**, 61, 119.
- [22] a) W. Luo, Y. Gong, Y. Zhu, K. K. Fu, J. Dai, S. D. Lacey, C. Wang, B. Liu, X. Han, Y. Mo, E. D. Wachsman, L. Hu, *J. Am. Chem. Soc.* **2016**, 138, 12258; b) X. Xiang, Y. Zhang, H. Wang, C. Wei, F. Chen, Q. Shen, *J. Electrochem. Soc.* **2021**, 168, 060515; c) R. Dubey, J. Sastre, C. Cancellieri, F. Okur, A. Forster, L. Pompizii, A. Priebe, Y. E. Romanyuk, L. P. H. Jeurgens, M. V. Kovalenko, K. V. Kravchyk, *Adv. Energy Mater.* **2021**, 11, 2102086; d) Y. Ruan, Y. Lu, X. Huang, J. Su, C. Sun, J. Jin, Z. Wen, *J. Mater. Chem. A* **2019**, 7, 14565; e) C. Cui, Q. Ye, C. Zeng, S. Wang, X. Xu, T. Zhai, H. Li, *Energy Storage Mater.* **2022**, 45, 814; f) G. Yang, Y. Zhang, Z. Guo, C. Zhao, X. Bai, L. Fan, N. Zhang, *Electrochim. Acta* **2022**, 407, 139767.
- [23] a) C. Wang, H. Xie, W. Ping, J. Dai, G. Feng, Y. Yao, S. He, J. Weaver, H. Wang, K. Gaskell, L. Hu, *Energy Storage Mater.* **2019**, 17, 234; b) H. Huo, X. Li, Y. Sun, X. Lin, K. Doyle-Davis, J. Liang, X. Gao, R. Li, H. Huang, X. Guo, X. Sun, *Nano Energy* **2020**, 73, 104836.
- [24] S.-K. Otto, Y. Moryson, T. Krauskopf, K. Peppeler, J. Sann, J. Janek, A. Henss, *Chem. Mater.* **2021**, 33, 859.
- [25] R. Schmuck, R. Wagner, G. Hörpel, T. Placke, M. Winter, *Nat. Energy* **2018**, 3, 267.
- [26] J. Wang, H. Wang, J. Xie, A. Yang, A. Pei, C.-L. Wu, F. Shi, Y. Liu, D. Lin, Y. Gong, Y. Cui, *Energy Storage Mater.* **2018**, 14, 345.
- [27] K. Kanamura, H. Tamura, S. Shiraishi, Z. i. Takehara, *J. Electrochem. Soc.* **1995**, 142, 340.
- [28] a) J. Meng, Y. Zhang, X. Zhou, M. Lei, C. Li, *Nat. Commun.* **2020**, 11, 3716; b) W. Luo, Y. Gong, Y. Zhu, Y. Li, Y. Yao, Y. Zhang, K. Fu, G. Pastel, C.-F. Lin, Y. Mo, E. D. Wachsman, L. Hu, *Adv. Mater.* **2017**, 29, 1606042; c) W. Feng, X. Dong, Z. Lai, X. Zhang, Y. Wang, C. Wang, J. Luo, Y. Xia, *ACS Energy Lett.* **2019**, 4, 1725.
- [29] a) M. Kotobuki, K. Kanamura, Y. Sato, T. Yoshida, *J. Power Sources* **2011**, 196, 7750; b) K. H. Kim, T. Hirayama, C. A. J. Fisher,

- K. Yamamoto, T. Sato, K. Tanabe, S. Kumazaki, Y. Iriyama, Z. Ogumi, *Mater. Charact.* **2014**, *91*, 101.
- [30] a) Y. Li, X. Chen, A. Dolocan, Z. Cui, S. Xin, L. Xue, H. Xu, K. Park, J. B. Goodenough, *J. Am. Chem. Soc.* **2018**, *140*, 6448; b) M. He, Z. Cui, C. Chen, Y. Li, X. Guo, *J. Mater. Chem. A* **2018**, *6*, 11463.
- [31] a) X. Ma, Y. Xu, *Electrochim. Acta* **2022**, *409*, 139986; b) K. Lee, S. Han, J. Lee, S. Lee, J. Kim, Y. Ko, S. Kim, K. Yoon, J.-H. Song, J. H. Noh, K. Kang, *ACS Energy Lett.* **2022**, *7*, 381; c) X. He, F. Yan, M. Gao, Y. Shi, G. Ge, B. Shen, J. Zhai, *ACS Appl. Mater. Interfaces* **2021**, *13*, 42212.
- [32] L. Zhuang, X. Huang, Y. Lu, J. Tang, Y. Zhou, X. Ao, Y. Yang, B. Tian, *Ceram. Int.* **2021**, *47*, 22768.
- [33] N. D. Lepley, N. A. W. Holzwarth, *Phys. Rev. B* **2015**, *92*, 214201.
- [34] X. Jin, Z. Cai, X. Zhang, J. Yu, Q. He, Z. Lu, M. Dahbi, J. Alami, J. Lu, K. Amine, H. Zhang, *Adv. Mater.* **2022**, *34*, 2200181.